THE JOURNAL OF PHYSICAL CHEMISTRY Letters

Letter

pubs.acs.org/JPCL

Patterning Graphitic C–N Sheets into a Kagome Lattice for Magnetic Materials

Xiaowei Li,[†] Jian Zhou,[‡] Qian Wang,*[,†,§] Yushiyuki Kawazoe,[⊥] and Puru Jena[§]

[†]Center for Applied Physics and Technology and [‡]Department of Materials Science and Engineering, College of Engineering, Peking University, Beijing 100871, China

[§]Department of Physics, Virginia Commonwealth University, Richmond, Virginia 23284, United States

[⊥]Institute for Material Research, Tohoku University, Sendai 980-8577, Japan

ABSTRACT: We propose porous C–N-based structures for biocompatible magnetic materials that do *not* contain even a single metal ion. Using first-principles calculations based on density functional theory, we show that when patterned in the form of a kagome lattice, nonmagnetic g-C_3N_4 not only becomes ferromagnetic but also its magnetic properties can be further enhanced by applying external strain. Similarly, the magnetic moment per atom in ferromagnetic g-C_4N_3 is increased three fold when patterned into a kagome lattice. The Curie temperature of g-C_3N_4 kagome lattice is 100 K, while that of g-C_4N_3 kagome lattice is much higher, namely, 520 K. To date, all of the synthesized two- and three-dimensional magnetic kagome structures contain metal ions and are toxic. The objective of our work is to stimulate an experimental effort to develop nanopatterning techniques for the synthesis of g-C_3N_4- and g-C_4N_3-based kagome lattices.

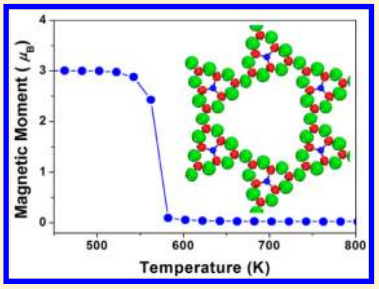

SECTION: Surfaces, Interfaces, Porous Materials, and Catalysis

Magnetic materials without metals are hotly pursued for their potential applications as biocompatible magnetic materials. Unlike conventional magnetic materials where magnetism is due to d or f electrons, the magnetic materials based on nonmetal p electrons have weak spin–orbit coupling and hyperfine interaction, which are the main channels of relaxation and decoherence of electron spins. Mn atoms, because of their special electronic configuration of $3d^5 4s^2$ and large magnetic moment of 5 μ_B, have been widely used as a dopant in various semiconductors such as GaAs, GaN, ZnO, AlN, and SiC. However, Mn is neurotoxic; both Mn^{2+} and Mn^{3+} can enter the brain by crossing the blood–brain barrier and cause permanent neurological disorder with symptoms similar to those of Parkinson's disease, including tremors, difficulty in walking, and facial muscle spasms.[1,2] In fact, most metal ions are toxic. Therefore, for biocompatibility, magnetic materials without metals are highly desirable. It is well-known that 3d electrons of transition-metal atoms can introduce magnetism, as do 2p electrons in some nonmetal atoms. Although 3d and 2p electrons have different orbital shapes, they share similar features in their radial distribution. Therefore, in some bonding environments, 2p electrons can display magnetism, as demonstrated in carbon nanostructures.[3] Unfortunately, some carbon nanostructures are not biocompatible either. For example, carbon nanotubes injected into the mouse's trachea induce severe granulomatous and lung inflammation.[4] However, when nitrogen-doped carbon nanotubes are used, biocompatibility improves significantly,[4] and these materials can be further used as biomembranes.[5] These findings suggest that magnetic materials composed of C and N are highly promising for applications in spintronics as well as in biotechnology.

A great deal of experimental effort has been devoted in this direction, leading to the synthesis of graphitic C_3N_4[6,7] and C_4N_3.[8] There are two types of structural isomers of g-C_3N_4; they consist of s-triazine units (ring of C_3N_3) or tri-s-triazine units (tri-ring of C_6N_7), respectively. We use both of them to construct kagome structures. Although increased attention has been paid to g-C_3N_4 for applications in fuel cells, photocatalysis, and hydrogen production,[9−16] no study has been reported for its applications as a magnetic material. We wondered if the nonferromagnetic g-C_3N_4[17] can be made ferromagnetic without introducing any metal ion. Recently, g-C_4N_3 was found to exhibit ferromagnetism,[18] providing a pathway for the design and synthesis of C–N-based magnetic materials. Can the magnetic properties of g-C_4N_3 be further enhanced by patterning it into a kagome lattice? In this study, we show that these can indeed be achieved when g-C_3N_4 (consisting of tri-s-triazine units) and g-C_4N_3 are patterned into kagome-lattice-type configurations, namely, a lattice pattern composed of interlaced triangles with shared vertices (Figure 1). Kagome lattice, which originally means a bamboo-basket (kago) woven pattern (me), is a well-known mathematical model for frustrated magnetism.[19−21] It has recently been found that this kind of structure has exceptional mechanical properties.[22,23] So far, the commonly used methods for synthesis of 2D kagome structures are based on bottom-up strategies, for

Received: November 17, 2012
Accepted: December 26, 2012
Published: December 26, 2012

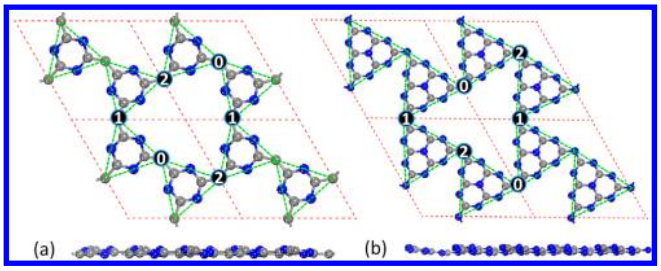

Figure 1. Schematic geometries of (a) g-C_4N_3- and (b) g-C_3N_4-based kagome lattices with top and side views. The TNF is marked by green dashed lines. The numbers represent the shift directions of the linking atoms. 1: upward; 2: downward; 0: in plane. Blue and gray balls represent N and C atoms, respectively. One unit cell is marked by a red dashed rhombus.

example, using metal−organic coordination or supramolecular self-assembly of specific molecules on the surface of substrates.[24,25] The physical synthesis based on the top-down method is also found to be possible by using electron beam irradiation, etching techniques,[26,27] lithography,[28] or nanocutting,[29] as demonstrated in a graphene sheet. In the following, we present our findings of the enhanced magnetism in g-C_4N_3 and induced magnetism in g-C_3N_4-based kagome structures.

All calculations were performed by using spin-polarized density functional theory (DFT) as implemented in the Vienna ab initio simulation package (VASP code).[30] Electronic exchange and correlation effects were treated using the generalized gradient approximation (GGA) with Perdew−Burke−Ernzerhof (PBE) parametrization.[31] The interactions between electrons and nuclei were treated using projector-augmented wave (PAW) potentials. Hybrid functionals using the Heyd−Scuseria−Ernzerhof (HSE06) form[32] were also used to achieve greater accuracy of the magnetic and electronic properties. The energy cutoff was set at 400 eV. The convergence criteria for energy and force were set to 0.01 meV and 0.001 eV/Å, respectively. The Brillouin zones were represented by Γ-centered unit cells with 11 × 11 × 1 Monkhorst−Pack special k-point mesh for a g-C_4N_3- and 7 × 7 × 1 mesh for a g-C_3N_4-based kagome lattice, respectively. The vacuum space in the nonperiodic direction is taken to be 15 Å, which is sufficient to avoid the interaction between the two neighboring images. In order to study the magnetic coupling between the two kagome sites or linking atoms, a supercell consisting of a 2 × 2 unit cell was used. The energy difference ΔE between the ferromagnetic (FM) and antiferromagnetic (AFM) or nonmagnetic (NM) states, defined as $\Delta E = E_{AFM(NM)} - E_{FM}$, was calculated to determine the magnetic ground state. Noncollinear spin calculations were performed to study possible spin canting, but spins were found to be collinear. Monte Carlo simulations involving 5×10^9 steps and a (100 × 100) supercell were further carried out to study magnetism at finite temperatures.

The geometric structures of g-C_4N_3- and g-C_3N_4-based kagome lattices are shown in Figure 1, where the triangular nanoflakes (TNFs) are linked by carbon or nitrogen atoms, respectively. Compared with the original g-C_4N_3 and g-C_3N_4 sheets, the corresponding kagome lattices are more porous. In order to investigate the stability of the kagome lattices, larger supercells consisting of 3 × 3 and 2 × 2 unit cells were used, respectively, for g-C_4N_3- and g-C_3N_4-based kagome lattices, and spin-polarized ab initio molecular dynamics simulations were performed at room temperature (300 K) with a time step of 1 fs. After 5000 steps, the frameworks are still intact, and the magnetic moments remain 54 μ_B for 3 × 3 unit cells or 12 μ_B for 2 × 2 unit cells. When annealed from 300 to 0 K, some atoms in g-C_4N_3- and g-C_3N_4-based kagome lattices exhibit slight buckling along the z direction, indicating that they are not strictly flat. The shift of some atoms in the deformed g-C_4N_3- and g-C_3N_4-based kagome lattices is less than 0.20 and 0.38 Å, respectively, and the corresponding total energy is 0.082 or 0.075 eV/unit cell lower than that of the planar structures. The top and side views of fully relaxed structures with deformations are shown in Figure 1. Note that some linking atoms are shifted upward or downward from the plane (labeled with 1 and 2) and that some linking atoms remain in the plane (labeled with 0). For the deformed structures, phonon calculations at the Γ point did not reveal any unstable modes. In the following, we discuss the properties of these deformed structures.

The lattice constants of g-C_4N_3- and g-C_3N_4-based kagome lattices are calculated to be 9.0 and 11.7 Å, respectively. The angle between the linking atom and its nearest two C atoms of the g-C_4N_3-based kagome lattice is found to be 142.2−142.4°, which is larger than that of the g-C_3N_4-based kagome lattice (115.1−115.3°). Figure 2a and b presents the 3D isosurface of

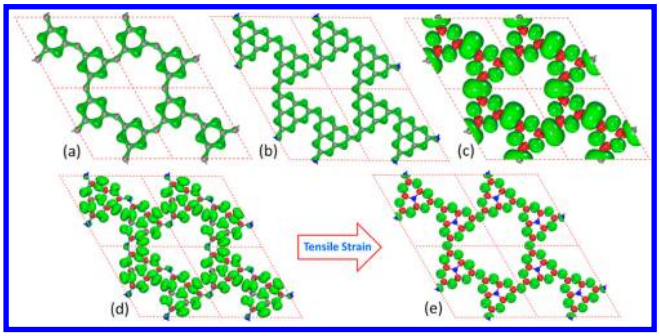

Figure 2. Isosurfaces of charge density with 1.8 e Å^{-3} of (a) g-C_4N_3- and (b) g-C_3N_4-based kagome lattices and spin density with 0.01 μ_B Å^{-3} of (c) a g-C_4N_3-based kagome lattice and (d and e) g-C_3N_4-based kagome lattices without and with tensile strain of 12.6%. The green and red colors in (c−e) represent the spin-up and spin-down electrons, respectively.

charge distribution for g-C_4N_3- and g-C_3N_4-based kagome lattices. We see that N atoms carry more charges due to their larger electron affinity. Comparing the charges located on the linking atoms and those on the TNF atoms, we observe that the linking C atoms carry slightly less charge (2.44 e) than the other C atoms (2.59 e) by 0.14 electrons. On the other hand, for the g-C_3N_4-based kagome lattice, the electrons (3.90 e) at the linking nitrogen atoms are approximately the same as that in the three- (two-)coordinated N atoms in the tri-s-triazine units, namely, 3.92 (3.86) electrons.

The ground state of the g-C_4N_3-based kagome lattice was found to be ferromagnetic, which is lower in energy by 0.22 and 0.92 eV/unit cell than that of the AFM and NFM states, respectively. The total magnetic moment per one unit cell is 6.0 μ_B (or 0.400 μ_B/atom). We note that the magnetic moment of pristine g-C_4N_3 is 1.0 μ_B/unit cell, or 0.14 μ_B/atom.[18] The underlying reason for the enhancement of the magnetic moment is that the original g-C_4N_3 consists of two-coordinated N and three-coordinated C, while in the kagome structure, the three-coordinated linking C atoms become two-coordinated. This change in coordination increases the magnetic moment

dx.doi.org/10.1021/jz3018804 | J. Phys. Chem. Lett. 2013, 4, 259−263

especially on the linking C sites, as shown in Figure 2c, and these linking C atoms with an enhanced magnetic moment act as a mediator of the magnetic coupling between the TNFs, resulting in an enhanced magnetic stability as compared to that of the original g-C_4N_3 structure.[18]

To get a better understanding of this system, the band structures and partial densities of states (PDOS) are given in Figure 3. We see that the system becomes an indirect band gap

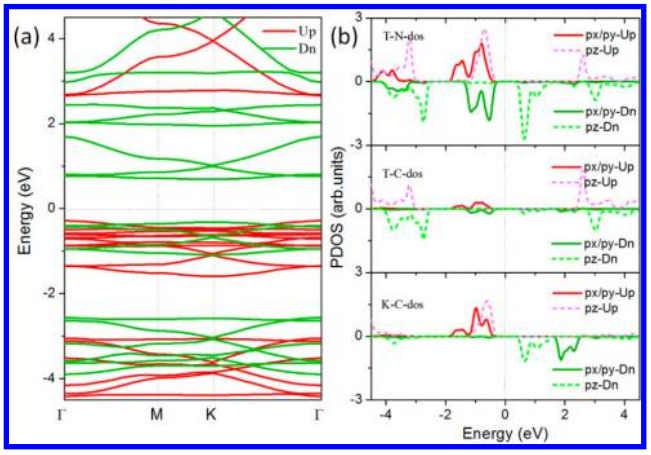

Figure 3. (a) Band structure and (b) partial DOS of p (p_x, p_y, p_z) orbitals of a g-C_4N_3-based kagome lattice. T-N-dos, T-C-dos, and K-C-dos indicate the partial DOS from N and C atoms in TNFs and C atoms at the linking sites in one unit cell. Up and Dn represent spin-up and spin-down, respectively. The Fermi level is shifted to zero.

semiconductor with an energy band gap of 1.2 eV. The N sites are ferromagnetically polarized (see Figure 2c), and the main contribution is from the N $2p_z$ orbitals (labeled as T-N in Figure 3b). The p_x, p_y, and p_z states of the linking C sites (labeled as K-C), are highly polarized and different from those of the inner C sites (labeled as T-C), which are negatively polarized. Near the Fermi level, there are six split energy bands dominated by the p_z orbitals of T-N and the p_x, p_y, and p_z orbitals of K-C.

To further examine the magnetic properties of the g-C_4N_3-based kagome lattice at finite temperatures, Monte Carlo simulations are carried out by using the Ising model Hamiltonian, $(H = (-\sum_{\langle i,j\rangle} J_{ij}s_is_j))$, where i and j represent two nearest-neighbor magnetic sites. The exchange parameter J can be derived from the energy difference between the FM and AFM states. Using the Ising model, we estimate $E_{FM} = -6Js^2$ and $E_{AFM} = 2Js^2$ in one unit cell, where s represents the magnetic moment of the linking C atoms, which is 2 μ_B. Thus, we have $J = (E_{AFM} - E_{FM})/8s^2 = 6.9$ meV. The variation of magnetic moment per unit cell with respect to temperature is plotted in Figure 4. We note that the magnetic moment remains in the high spin state in the low-temperature range and then drops to near zero at the Curie temperature of 520 K. This clearly indicates that ferromagnetism in the g-C_4N_3-based kagome lattice can be detected at room temperature. This is consistent with our previous molecular dynamics simulation.

The exceptional magnetic properties observed in the g-C_4N_3-based kagome lattice motivated us to explore the magnetism in the g-C_3N_4-based kagome structure. We found that the g-C_3N_4-based kagome structure, composed of s-triazine units, is nonmagnetic, while the kagome lattice consisting of tri-s-triazine units is ferromagnetic, which is lower in energy than the AFM (NM) state by 0.03 (0.33) eV/unit cell. The spin density

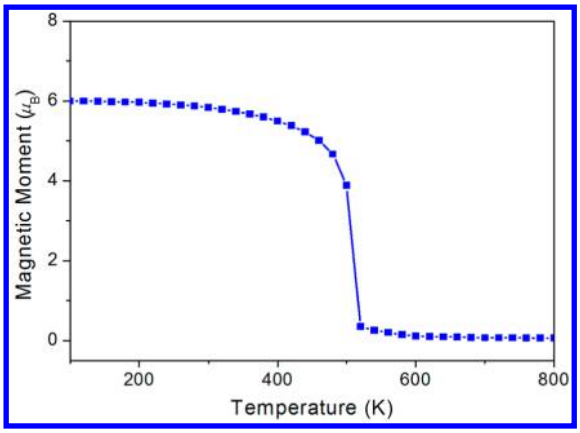

Figure 4. Variation of magnetization per unit cell with respect to temperature of the g-C_4N_3-based kagome lattice.

isosurface for the FM state is given in Figure 2d. In one unit cell, the magnetic moment is 3.0 μ_B, which mainly comes from the p_x and p_y orbitals of N atoms in the TNFs (labeled as T-N in Figure 5b), while all of the C sites and the linking N atoms at

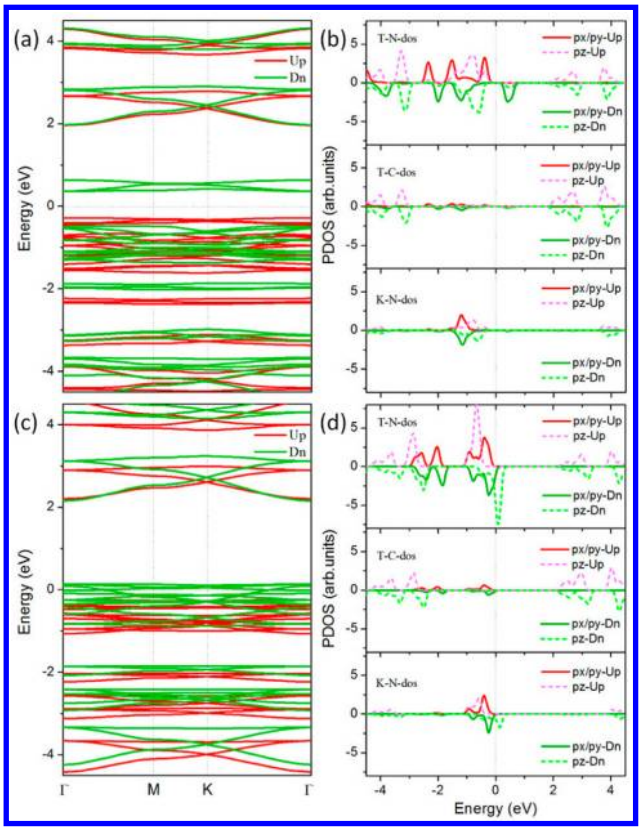

Figure 5. The legend is similar to that in Figure 3. (a,b) Unstrained g-C_3N_4-based kagome lattice. (c,d) Strained (12.6%) g-C_3N_4-based kagome lattice.

the kagome sites are weakly spin-polarized. The system becomes an indirect band gap semiconductor with a small gap of 0.6 eV (see Figure 5a).

From the above, we see that the original nonmagnetic g-C_3N_4 becomes magnetic when it is patterned into the kagome lattice, but the energy difference between the FM and AFM is small (only 0.03 eV/unit cell). A similar procedure of estimating the exchange parameter can be applied here, and

dx.doi.org/10.1021/jz3018804 | J. Phys. Chem. Lett. 2013, 4, 259−263

we find that $J = (E_{AFM} - E_{FM})/8s^2 = 3.8$ meV because $s = 1\ \mu_B$ in the present case. The corresponding Curie temperature is calculated to be 100 K, which is far below room temperature. In the following, we discuss the possible approach to improve the stability of the FM state. We know that there are two main factors affecting magnetism, coordination number and bond length. To maintain the skeleton of g-C_3N_4 and to keep the feature of the kagome lattice, the coordination number cannot be reduced any further. However, it is possible to increase the bond length by applying tensile strain. We define the biaxial tensile strain as $(L - L_0)/L_0$*100%, where L_0 ($L_1 = L_2 = L_0$) and L are the lattice constants of the g-C_3N_4-based kagome lattice in equilibrium and in strained states, respectively. We found that tensile strain can enhance the stability of the FM state. For example, when the tensile strain reaches 12.6%, the energy difference between the FM and AFM states increases sharply from 0.03 to 0.15 eV/unit cell. During the tension, the angle between the linking atom and its nearest two C atoms of the g-C_3N_4-based kagome lattice increases significantly, but the bond length of C−N is only slightly enlarged (<0.03 Å) without breaking, which suggests that the system can endure such strain. Furthermore, the energy and in-plane tension required to reach such a biaxial strain value is found to be 1.2 eV and 1.9 GPa·nm, respectively, indicating that such a strain state can be achieved experimentally. In this strain state, the exchange parameter using the FM and AFM state energies is expressed as $J = (E_{AFM} - E_{FM})/8s^2 = 18.8$ meV. After Monte Carlo simulations, the Curie temperature increases to 580 from 100 K. The corresponding spin density isosurface is shown in Figure 2e. The most notable change is that the magnetic moments at the linking N and C sites in TNF are significantly enhanced, which improves the ferromagnetic coupling between the magnetic units. The main contribution to the moment arises from N p_z orbitals. The band structure and DOS (Figure 5c and d) further show that the system becomes a semimetal with semiconducting spin-up and metallic spin-down channels. This suggests that the strain manipulation can effectively modify the magnetism as well as the electronic structure.

To further confirm our main results, we used the HSE06 hybrid functional, which has been proved to be more accurate. We found that the ground states are still ferromagnetic with the same magnetic moment and the same spin split orbitals, as discussed above. Different from the PBE results, all conduction bands are shifted upward. Correspondingly, the band gaps of g-C_4N_3- and g-C_3N_4-based kagome lattices are increased to 2.6 and 1.7 eV, respectively. In the g-C_3N_4-based kagome lattice with a tensile strain of 12.6%, the valence bands occupied by p_x and p_y orbitals are downshifted, while the spin-down p_z orbitals cross the Fermi surface (as shown in Figure 6), similar to the results shown in Figure 5c and d, confirming again that the strained system is a semimetal.

In summary, on the basis of spin-polarized DFT, we show that when patterned into kagome structures, the nonmagnetic g-C_3N_4 becomes ferromagnetic, and the magnetism of g-C_4N_3 can be enhanced, where the Curie temperature becomes 520 K and the magnetic moment per unit cell increases three-fold. These kagome structures can be fabricated using electron beam irradiation, etching techniques,[26,27] lithography,[28] or nanocutting[29] developed for graphene. The resulting 2D kagome structures show some advantages over the existing systems synthesized by using a metal−organic coordination network or supramolecular self-assembly of specific molecules on the surface of substrates, where metal ions are used to induce magnetism. Accordingly, its biocompatibility is compromised. Our studied systems with enhanced magnetism, porosity, and biocompatibility are promising candidates for applications in medicine and spintronics.

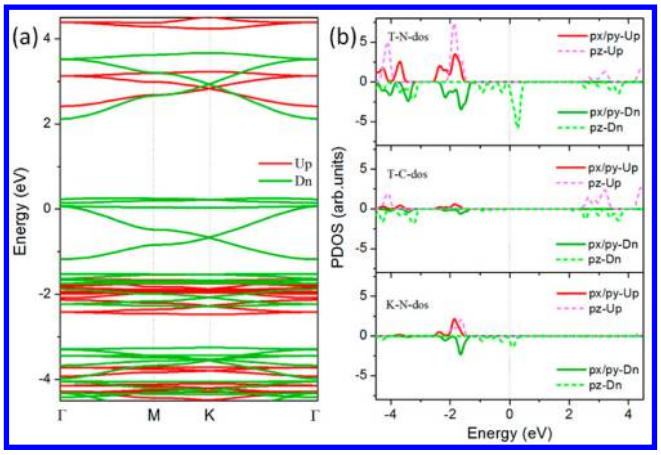

Figure 6. The legend is similar to that in Figure 3. (a) Band structures and (b) partial DOS calculated by the HSE06 functional for the g-C_3N_4-based kagome lattice with a tensile strain of 12.6%.

AUTHOR INFORMATION

Corresponding Author

*E-mail: qianwang2@pku.edu.cn.

Notes

The authors declare no competing financial interest.

ACKNOWLEDGMENTS

This work is supported by grants from the National Natural Science Foundation of China (Grants NSFC-11174014 and NSFC-21273012) and the National Grand Fundamental Research 973 Program of China (Grant 2012CB921404). X.L. acknowledges support from the China Postdoctoral Science Foundation (Grant 2012M510246). The work is partially supported by JST, CREST, "A mathematical challenge to a new phase of material sciences" (2008−2013), and the support is genuinely and sincerely appreciated. P.J. acknowledges partial support from the Department of Energy.

REFERENCES

(1) Aschner, M.; Gannon, M. Manganese (Mn) Transport Across the Rat Blood−Brain Barrier: Saturable and Transferrin-dependent Transport Mechanisms. *Brain Res. Bull.* **1994**, *33*, 345−349.

(2) Murphy, V. A.; Wadhwani, K. C.; Smith, Q. R.; Rapoport, S. I. Saturable Transport of Manganese(II) Across the Rat Blood−Brain Barrier. *J. Neurochem.* **1991**, *57*, 948−954.

(3) Zhou, J.; Wang, Q.; Sun, Q.; Jena, P. Intrinsic Ferromagnetism in Two-Dimensional Carbon Structures: Triangular Graphene Nanoflakes Linked by Carbon Chains. *Phys. Rev. B* **2011**, *84*, 081402(R).

(4) Carrero-Sánchez, J. C.; Elías, A. L.; Mancilla, R.; Arrellín, G.; Terrones, H.; Laclette, J. P.; Terrones, M. Biocompatibility and Toxicological Studies of Carbon Nanotubes Doped with Nitrogen. *Nano Lett.* **2006**, *6*, 1609−1616.

(5) Yang, Y.; Li, X.; Jiang, J.; Du, H.; Zhao, L.; Zhao, Y. Control Performance and Biomembrane Disturbance of Carbon Nanotube Artificial Water Channels by Nitrogen-Doping. *ACS Nano* **2010**, *4*, 5755−5762.

(6) Döblinger, M.; Lotsch, B. V.; Wack, J.; Thun, J.; Senker, J.; Schnick, W. Structure Elucidation of Polyheptazine Imide by Electron Diffraction — A Templated 2D Carbon Nitride Network. *Chem. Commun.* **2009**, 1541−1543.

(7) Wang, X.; Maeda, K.; Chen, X.; Takanabe, K.; Domen, K.; Hou, Y.; Fu, X.; Antonietti, M. Polymer Semiconductors for Artificial Photosynthesis: Hydrogen Evolution by Mesoporous Graphitic Carbon Nitride with Visible Light. *J. Am. Chem. Soc.* **2009**, *131*, 1680−1681.
(8) Lee, J. S.; Wang, X. Q.; Luo, H. M.; Dai, S. Fluidic Carbon Precursors for Formation of Functional Carbon under Ambient Pressure Based on Ionic Liquids. *Adv. Mater.* **2010**, *22*, 1004−1007.
(9) Wang, Y.; Wang, X.; Antonietti, M. Polymeric Graphitic Carbon Nitride as a Heterogeneous Organocatalyst: From Photochemistry to Multipurpose Catalysis to Sustainable Chemistry. *Angew. Chem., Int. Ed.* **2012**, *51*, 68−89.
(10) Wang, X.; Blechert, S.; Antonietti, M. Polymeric Graphitic Carbon Nitride for Heterogeneous Photocatalysis. *ACS Catal.* **2012**, *2*, 1596−1606.
(11) Zheng, Y.; Liu, J.; Liang, J.; Jaroniec, M.; Qiao, S. Z. Graphitic Carbon Nitride Materials: Controllable Synthesis and Applications in Fuel Cells and Photocatalysis. *Energy Environ. Sci.* **2012**, *5*, 6717−6731.
(12) Ge, L.; Zuo, F.; Liu, J.; Ma, Q.; Wang, C.; Sun, D.; Bartels, L.; Feng, P. Synthesis and Efficient Visible Light Photocatalytic Hydrogen Evolution of Polymeric g-C_3N_4 Coupled with CdS Quantum Dots. *J. Phys. Chem. C* **2012**, *116*, 13708−13714.
(13) Min, S.; Lu, G. Enhanced Electron Transfer from the Excited Eosin Y to mpg-C_3N_4 for Highly Efficient Hydrogen Evolution under 550 nm Irradiation. *J. Phys. Chem. C* **2012**, *116*, 19644−19652.
(14) Niu, P.; Liu, G.; Cheng, H. Nitrogen Vacancy-Promoted Photocatalytic Activity of Graphitic Carbon Nitride. *J. Phys. Chem. C* **2012**, *116*, 11013−11018.
(15) Xiang, Q.; Yu, J.; Jaroniec, M. Preparation and Enhanced Visible-Light Photocatalytic H_2-Production Activity of Graphene/C_3N_4 Composites. *J. Phys. Chem. C* **2011**, *115*, 7355−7363.
(16) Sehnert, J.; Baerwinkel, K.; Senker, J. Ab Initio Calculation of Solid-State NMR Spectra for Different Triazine and Heptazine Based Structure Proposals of g-C_3N_4. *J. Phys. Chem. B* **2007**, *111*, 10671−10680.
(17) Du, A.; Sanvito, S.; Li, Z.; Wang, D.; Jiao, Y.; Liao, T.; Sun, Q.; Ng, Y. H.; Zhu, Z.; Amal, R.; Smith, S. C. Hybrid Graphene and Graphitic Carbon Nitride Nanocomposite: Gap Opening, Electron−Hole Puddle, Interfacial Charge Transfer, and Enhanced Visible Light Response. *J. Am. Chem. Soc.* **2012**, *134*, 4393−4397.
(18) Du, A.; Sanvito, S.; Smith, S. C. First-Principles Prediction of Metal-Free Magnetism and Intrinsic Half-Metallicity in Graphitic Carbon Nitride. *Phys. Rev. Lett.* **2012**, *108*, 197207.
(19) Wang, X. Y.; Wang, L.; Wang, Z. M.; Gao, S. Solvent-Tuned Azido-Bridged Co^{2+} Layers: Square, Honeycomb, and Kagomé. *J. Am. Chem. Soc.* **2006**, *128*, 674−675.
(20) Schweika, W.; Valldor, M.; Lemmens, P. Approaching the Ground State of the Kagome Antiferromagnet. *Phys. Rev. Lett.* **2007**, *98*, 067201.
(21) Aidoudi, F. H.; Aldous, D. W.; Goff, R. J.; Slawin, A. M. Z.; Attfield, J. P.; Morris, R. E.; Lightfoot, P. An Ionothermally Prepared *S* = 1/2 Vanadium Oxyfluoride Kagome Lattice. *Nat. Chem.* **2011**, *3*, 801−806.
(22) Sun, K.; Souslov, A.; Mao, X.; Lubensky, T. C. Surface Phonons, Elastic Response, and Conformal Invariance in Twisted Kagome Lattices. *Proc. Natl. Acad. Sci. U.S.A.* **2012**, *109*, 12369−12374.
(23) Vitelli, V. Topological Soft Matter: Kagome Lattices with a Twist. *Proc. Natl. Acad. Sci. U.S.A.* **2012**, *109*, 12266−12267.
(24) Mao, J.; Zhang, H.; Jiang, Y.; Pan, Y.; Gao, M.; Xiao, W.; Gao, H.-J. Tunability of Supramolecular Kagome Lattices of Magnetic Phthalocyanines Using Graphene-Based Moiré Patterns as Templates. *J. Am. Chem. Soc.* **2009**, *131*, 14136−14137.
(25) Chen, Q.; Bae, S. C.; Granick, S. Directed Self-Assembly of a Colloidal Kagome Lattice. *Nature* **2011**, *469*, 381−384.
(26) Jin, C.; Lan, H.; Peng, L.; Suenaga, K.; Iijima, S. Deriving Carbon Atomic Chains from Graphene. *Phys. Rev. Lett.* **2009**, *102*, 205501.
(27) Chuvilin, A.; Meyer, J. C.; Algara-Siller, G.; Kaiser, U. From Graphene Constrictions to Single Carbon Chains. *New J. Phys.* **2009**, *11*, 083019.
(28) Bai, J.; Zhong, X.; Jiang, S.; Huang, Y.; Duan, X. Graphene Nanomesh. *Nat. Nanotechnol.* **2010**, *5*, 190−194.
(29) Ci, L.; Xu, Z.; Wang, L.; Gao, W.; Ding, F.; Kelly, K. F.; Yakobson, B. I.; Ajayan, P. M. Controlled Nanocutting of Graphene. *Nano Res.* **2008**, *1*, 116−122.
(30) Kresse, G.; Furthmuller, J. Efficient Iterative Schemes for *Ab Initio* Total-Energy Calculations Using a Plane-Wave Basis Set. *Phys. Rev. B* **1996**, *54*, 11169−11186.
(31) Perdew, J. P.; Burke, K.; Ernzerhof, M. Generalized Gradient Approximation Made Simple. *Phys. Rev. Lett.* **1996**, *77*, 3865−3868.
(32) Heyd, J.; Scuseria, G. E.; Ernzerhof, M. Erratum: "Hybrid Functionals Based on a Screened Coulomb Potential" [*J. Chem. Phys.* *118*, 8207 (**2003**)]. *J. Chem. Phys.* **2006**, *124*, 219906.